


## Effective Landé factors of electrons and holes in lead chalcogenide nanocrystals

I. D. Avdeev <sup>1</sup>, S. V. Goupalov <sup>1,2,\*</sup> and M. O. Nestoklon <sup>1</sup>

<sup>1</sup>*Ioffe Institute, 194021 St. Petersburg, Russia*

<sup>2</sup>*Department of Physics, Jackson State University, Jackson, Mississippi 39217, USA*

 (Received 26 October 2022; revised 19 December 2022; accepted 5 January 2023; published 17 January 2023)

The Landé or  $g$  factors of charge carriers in solid state systems provide invaluable information about the response of quantum states to external magnetic fields and are key ingredients in the description of spin-dependent phenomena in nanostructures. We report on a comprehensive theoretical analysis of electron and hole  $g$  factors in lead chalcogenide nanocrystals. By combining symmetry analysis, atomistic calculations, and extended  $\mathbf{k} \cdot \mathbf{p}$  theory, we relate calculated linear-in-magnetic field energy splittings of confined electron states in nanocrystals to the intravalley  $g$  factors of the multivalley bulk materials, renormalized due to the quantum confinement. We demonstrate that this renormalization is correctly reproduced by analytical expressions derived in the framework of the extended  $\mathbf{k} \cdot \mathbf{p}$  model.

DOI: [10.1103/PhysRevB.107.035414](https://doi.org/10.1103/PhysRevB.107.035414)

### I. INTRODUCTION

Lead salt nanocrystals (NCs) are enjoying many practical applications in optoelectronics and photovoltaics [1–5]. New devices built on NCs are predicted to enter the market in the very near future [5–8]. All these devices are based on the emission or absorption of light by spatially confined electron-hole pairs.

Applications of NCs in the rapidly developing fields of spintronics and quantum computing [9–12] would be impossible without control over the spin state of localized carriers. Therefore, knowledge about carrier spin relaxation and dynamics as well as their Landé  $g$  factors becomes critically important. These properties have been widely studied for CdSe NCs. The exciton fine-structure relaxation dynamics was investigated in Refs. [13–15], electron and exciton  $g$  factors were measured, respectively, by time-resolved Faraday rotation [16–18] and single-dot magnetophotoluminescence spectroscopy [19,20], and carrier  $g$  factors were calculated within the tight-binding [21–23] and effective mass [24] methods.

In the meantime, analogous studies for lead salt NCs remain very scarce. Ultrafast exciton fine-structure relaxation dynamics was studied by Johnson *et al.* [25]. Turyanska *et al.* deduced exciton  $g$  factors of PbS NCs from magnetic field dependences of the photoluminescence circular polarization degree [26]. Schaller *et al.* measured the averaged exciton  $g$  factor in an ensemble of PbSe NCs in magnetic-circular dichroism experiments [27] and extracted small (compared to the bulk) values of exciton  $g$  factors changing from 5 to 2 with decreasing NC size. They also observed traces of fine-structure splitting which they were not able to resolve. They commented that the extraction of  $g$  factors from polarization measurements is impossible without detailed knowledge of

this fine structure. Single-NC spectroscopy in external magnetic fields was performed by Kim *et al.* [28].

Yet, an interpretation of these results is complicated by the multivalley band structure of lead salt compounds. Bulk lead salts have extrema of the conduction and valence bands at the four inequivalent  $L$  points of the Brillouin zone. The widely used  $\mathbf{k} \cdot \mathbf{p}$  theory [29] treats these  $L$  valleys independently. An external magnetic field leads to the Zeeman splittings of the electron and hole states characterized by certain magnetic quantum numbers intimately related to the spin degrees of freedom. Then the main effects of the quantum confinement are the renormalization of the Zeeman splittings and their sensitivity to the orientation of the magnetic field, which result in the renormalization and anisotropy of the carriers'  $g$  factors [30]. This kind of narrative is typical for nanostructures of II-VI and III-V compound semiconductors with band extrema at the  $\Gamma$  point of the Brillouin zone, and is adopted by the conventional, or independent-valley,  $\mathbf{k} \cdot \mathbf{p}$  theory developed for lead salt nanostructures [29]. This theory is formulated in terms of the longitudinal and transverse single-valley  $g$  factors [Fig. 1(a)].

However, in lead salt nanostructures, due to the intervalley scattering on the surface, the zero-field electron or hole states represent combinations of the states originating from different  $L$  valleys. Thus, all atomistic band-structure calculations, based on the symmetries of the underlying crystal lattice and overall structure, automatically take into account this alignment of the valley degrees of freedom [31,32]. The resulting zero-field states are classified with respect to irreducible representations of the symmetry group. Application of the external magnetic field further affects the spin degrees of freedom, but this narrative implies a completely different meaning and definition of the magnetic quantum numbers as compared to the single-valley case. Since, at weak magnetic fields, states characterized by different irreducible representations do not mix, the atomistic theories operate with the  $g$  factors associated with the corresponding irreducible representations [Fig. 1(c)].

\*serguei.goupalov@jsums.edu

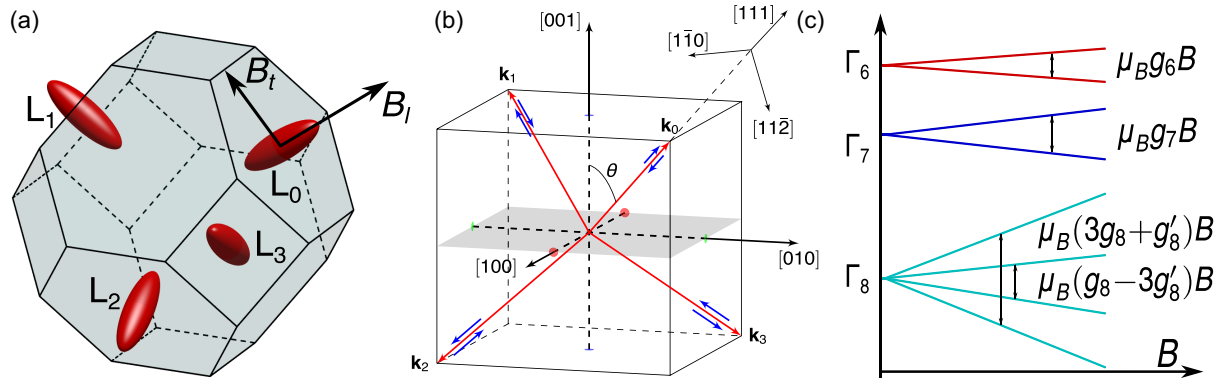


FIG. 1. (a) Conduction and valence band extrema in bulk lead chalcogenide compounds occur at four inequivalent  $L$  points of the Brillouin zone. Energy isosurfaces near these points form anisotropic valleys (red “cigars”). For the valley states of charge carriers, Zeeman splittings depend on the orientation of the magnetic field with respect to the valley main axes. One can distinguish longitudinal ( $B_l$ ) and transverse ( $B_t$ ) components of the magnetic field in a given valley which define the longitudinal ( $g_l$ ) and transverse ( $g_t$ )  $g$  factors. (b) Within the  $\mathbf{k} \cdot \mathbf{p}$  theory, projections of the total angular momentum  $F_z = \pm 1/2$  (blue arrows) are defined in the valley coordinate frames adjacent to the valley wave vectors  $\mathbf{k}_v$  (red arrows). These vectors form an irreducible star  $\{\mathbf{k}_0\}$  of some representation of the crystal space group [33]. One can analyze their transformation properties [34] and form combinations of valley states transforming under irreducible representations of the NC point group. This allows one to establish a relationship between the single-valley states described by the  $\mathbf{k} \cdot \mathbf{p}$  theory and the multivalley combinations of states in atomistic calculations, enforced by the microscopic symmetry of the NCs. (c) Zero-field states of charge carriers in NCs represent combinations of valley states transforming under certain irreducible representations of the NC point group. The ground electron (or hole) confinement level in a NC with no inversion center splits into two doublets and a quadruplet transforming under  $\Gamma_6$ ,  $\Gamma_7$ , and  $\Gamma_8$  irreducible representations of the group  $T_d$ . At low magnetic fields, the Zeeman splittings are isotropic and determined by four effective  $g$  factors  $g_6$ ,  $g_7$ ,  $g_8$ , and  $g'_8$ .

In this paper, we show that a solution to this ambiguity comes from a symmetry-based construction of a transformation relating the basis of independent valley states and the basis of valley combinations associated with certain irreducible representations of the point group, as illustrated in Fig. 1. This allows one to relate both kinds of  $g$  factors and use a fusion of the two approaches to get insight about the confinement effect on the carriers’  $g$  factors in lead salt NCs.

## II. RESULTS AND DISCUSSION

In  $\text{PbX}$  ( $X = \text{S, Se}$ ) NCs with cubic symmetry (point group  $T_d$  or  $O_h$ ) the ground state of the confined electron or hole splits into two doublets, transforming under irreducible representations  $\Gamma_6$ ,  $\Gamma_7$  ( $\Gamma_{6,7}^\pm$ ) of group  $T_d$  ( $O_h$ ), and a quadruplet  $\Gamma_8$  ( $\Gamma_8^\pm$ ) separated by several meV as a result of valley mixing [31,32,35,36]. In the subspace of these states, the interaction with a weak magnetic field  $\mathbf{B}$  is described by the following effective Hamiltonian, written as a block-diagonal matrix,

$$H_1^\eta(\mathbf{B}) = \mu_B \mathbf{B} \begin{pmatrix} \frac{1}{2}g_6^\eta \boldsymbol{\sigma} & 0 & 0 \\ 0 & \frac{1}{2}g_7^\eta \boldsymbol{\sigma} & 0 \\ 0 & 0 & g_8^\eta \mathbf{J} + g_8^{\prime\eta} \mathbf{J}' \end{pmatrix}, \quad (1)$$

where  $\eta = c(v)$  for the conduction- (valence-) band states;  $g_6^\eta$  and  $g_7^\eta$  are, respectively, the effective  $g$  factors of the  $\Gamma_6$  and  $\Gamma_7$  doublets;  $g_8^\eta$  and  $g_8^{\prime\eta}$  are the two constants describing Zeeman splitting of the quadruplet  $\Gamma_8$ ;  $\boldsymbol{\sigma} = (\sigma_x, \sigma_y, \sigma_z)$  are the Pauli matrices;  $\mathbf{J} = (J_x, J_y, J_z)$  are the matrices of the angular momentum  $j = 3/2$  [34],  $\mu_B$  is the Bohr magneton, and the matrices  $\mathbf{J}'$  are defined as [37]

$$J'_\gamma = \frac{5}{3}J_\gamma^3 - \frac{41}{12}J_\gamma \quad (2)$$

( $\gamma = x, y, z$ ).

In a strong magnetic field, when  $\mu_B B$  is compatible with the valley splittings  $|E_{\Gamma_7} - E_{\Gamma_8}|$  and  $|E_{\Gamma_8} - E_{\Gamma_6}|$ , two additional nondiagonal linear-in- $B$  terms should be taken into account. They describe the interaction of the quadruplet  $\Gamma_8$  with the doublets  $\Gamma_6$  and  $\Gamma_7$  and are discussed in the Supplemental Material [34].

### A. Tight-binding calculations

We follow the procedure described in Refs. [32,35,36] and use the extended tight-binding model [38] to compute the energies and wave functions of electron states in the conduction and valence bands for NCs of various shapes and classify them in accordance with irreducible representations of the point group  $T_d$  [36] (we restrict our consideration to stoichiometric NCs with no inversion center). We use the tight-binding parametrization from Ref. [32] which accurately reproduces the *ab initio* band structure from Ref. [39] corrected for experimental masses. The effect of the magnetic field is taken into account using the standard procedure of Ref. [40].

From the energy splittings induced by the external magnetic field we extract the constants in the effective Hamiltonian (1). They are shown in Fig. 2 for quasispherical PbS and PbSe NCs (see Supplemental Material [34] for a definition of quasispherical NCs). The actual shapes of colloidal NCs can vary from a cube to a truncated cube to a cuboctahedron to a truncated octahedron to an octahedron, depending on the synthesis conditions [41,42]. Tight-binding calculations performed for NCs of cubic, cuboctahedral, and octahedral shapes show that the  $g$  factors are almost shape independent, in contrast to the zero-field splittings of electron and hole levels exhibiting strong dependencies on the NC shape [36] (see

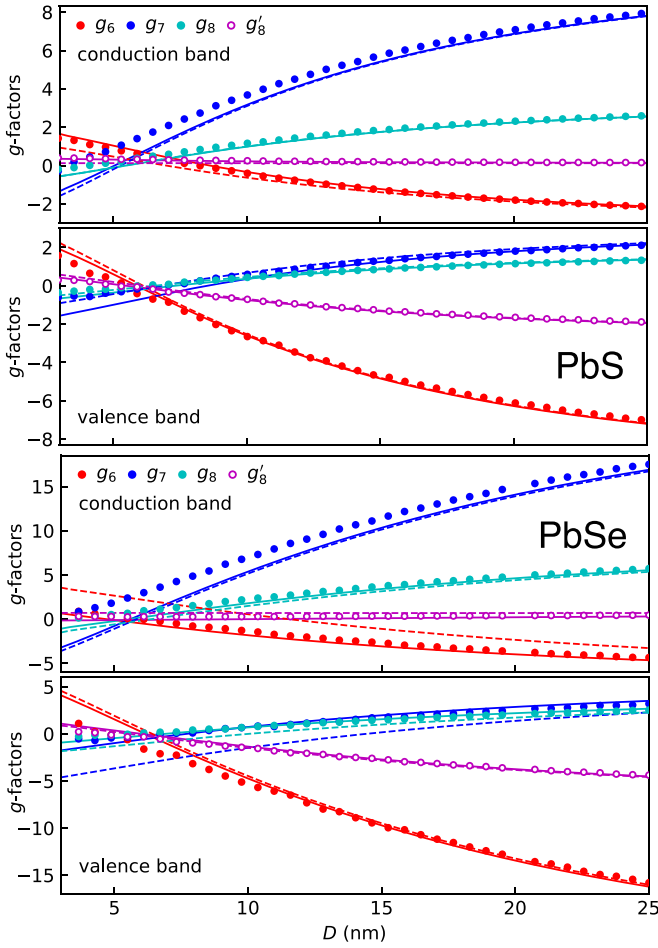


FIG. 2. Calculated  $g$  factors  $g_6$ ,  $g_7$ ,  $g_8$ , and  $g_8'$  (1) in conduction (top panel) and valence (second panel) bands of quasispherical PbS NCs (solid red, blue, cyan, and open purple circles, respectively). The results are stable with respect to NC shape variation, (see Supplemental Material [34]). Solid (dashed) lines show outcomes of the anisotropic (isotropic)  $\mathbf{k} \cdot \mathbf{p}$  model. The two lower panels show results for PbSe NCs.

Supplemental Material [34] for energies of the  $\Gamma_6$ ,  $\Gamma_7$ , and  $\Gamma_8$  levels in PbSe NCs; those for PbS NCs are given in Ref. [36]). By dashed (solid) lines in Fig. 2 we show the results of the isotropic (anisotropic)  $\mathbf{k} \cdot \mathbf{p}$  model to be discussed later.

### B. Landé factors in valleys

Before proceeding to the results of the  $\mathbf{k} \cdot \mathbf{p}$  model, we first discuss the origin of the parameters entering Eq. (1) in terms of anisotropic  $g$  factors describing the linear magnetic field dependence of the phenomenological single-valley effective Hamiltonians. We represent the Hamiltonian of the confined conduction- or valence-band ground state as a summation of the single-valley Hamiltonians over the valley index  $\nu$ ,

$$\hat{H}^\eta = \frac{\mu_B}{2} \sum_\nu [g_l^\eta (\sigma_x B_{x,\nu} + \sigma_y B_{y,\nu}) + g_t^\eta \sigma_z B_{z,\nu}], \quad (3)$$

where the Pauli matrices  $\sigma_\gamma$  ( $\gamma = x, y, z$ ) are defined in the coordinate frames of the corresponding valleys (with the  $z$  axis aligned along the valley  $C_3$  axis) and  $\mathbf{B} = (B_{x,\nu}, B_{y,\nu}, B_{z,\nu})$  is

the magnetic field written in the same “local” basis. In particular, for the  $L_0$  valley, we choose the local basis as follows:

$$\mathbf{n}_{x,0} \parallel [1\bar{1}0], \quad \mathbf{n}_{y,0} \parallel [11\bar{2}], \quad \mathbf{n}_{z,0} \parallel [111]. \quad (4)$$

The bases of the other valleys ( $\nu = 1, 2, 3$ ) are related via  $C_2$  rotations around the crystallographic axes of the “laboratory” frame ( $x \parallel [100]$ ,  $y \parallel [010]$ ,  $z \parallel [001]$ ):  $0 \rightarrow 1$  via  $C_{2x}$ ,  $0 \rightarrow 2$  via  $C_{2x}$ , and  $0 \rightarrow 3$  via  $C_{2y}$  [cf. Fig. 1(b)].

The Hamiltonian (3) can be transformed into the basis of irreducible representations using an appropriate transformation matrix [34]. From a comparison of the transformed Hamiltonian with Eq. (1) we obtain the following set of  $g$  factors for the confined conduction- and valence-band states:

$$g_6^c = \frac{g_l^c - 2g_t^c}{3}, \quad g_7^c = \frac{g_l^c + 2g_t^c}{3}, \quad (5a)$$

$$g_8^c = \frac{g_l^c + 4g_t^c}{15}, \quad g_8'^c = 2\frac{g_l^c - g_t^c}{15}, \quad (5b)$$

$$g_6^v = \frac{g_l^v + 2g_t^v}{3}, \quad g_7^v = \frac{g_l^v - 2g_t^v}{3}, \quad (5c)$$

$$g_8^v = \frac{g_l^v - 4g_t^v}{15}, \quad g_8'^v = 2\frac{g_l^v + g_t^v}{15}. \quad (5d)$$

Equations (5) can be inverted to extract the values of  $g_{l(t)}^\eta$  from the  $g$  factors of the quantum-confined states in a NC. We will use this procedure to obtain the effective  $g$  factors  $g_{l(t)}^{c(v)}$  from the tight-binding results presented in Fig. 2. One may notice that there are four independent constants for each band in the effective Hamiltonian (1) but only two independent constants entering (3). Therefore, we have some freedom in the choice of the extraction procedure. In the present study, we will determine the longitudinal and transverse  $g$  factors as

$$g_l^\eta = 3g_8^\eta + 6g_8'^\eta, \quad (6a)$$

$$g_t^\eta = 3g_8^\eta - \frac{3}{2}g_8'^\eta, \quad g_t^v = -3g_8^v + \frac{3}{2}g_8'^v. \quad (6b)$$

The longitudinal and transverse  $g$  factors obtained in this manner from the tight-binding calculations are presented in Fig. 3. Also shown in Fig. 3 are results of the single-valley  $\mathbf{k} \cdot \mathbf{p}$  model.

As the numbers of independent constants in Eqs. (1) and (3) are different, the above procedure introduces some error. In order to estimate it, in the Supplemental Material [34] we compare the difference between  $g_6^\eta$  and  $g_7^\eta$  calculated directly in the tight-binding with the results of Eqs. (5a) and (5c). The differences are correlated with the valley splittings and do not exceed 10% of the values of the  $g$  factors in the bulk.

### C. $\mathbf{k} \cdot \mathbf{p}$ model

It is well known [30] that quantum confinement renormalizes the electron  $g$  factor in semiconductor nanostructures with respect to its bulk counterpart. We will demonstrate the results of such a renormalization using the single-valley  $\mathbf{k} \cdot \mathbf{p}$  model of Ref. [29] (see also Refs. [43,44]). In the isotropic approximation, the effective Hamiltonian of this model can be written as

$$H_{\text{iso}} = \begin{pmatrix} \left(\frac{E_g}{2} - \alpha_c \Delta\right) & -\frac{i\hbar P}{m_0} (\boldsymbol{\sigma} \nabla) \\ -\frac{i\hbar P}{m_0} (\boldsymbol{\sigma} \nabla) & -\left(\frac{E_g}{2} - \alpha_v \Delta\right) \end{pmatrix}, \quad (7)$$

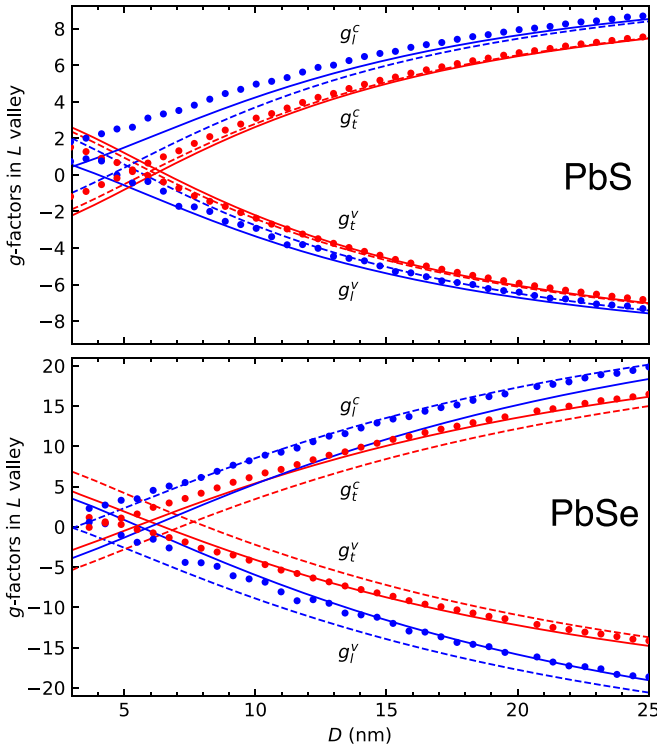


FIG. 3. The values of transverse (red circles) and longitudinal (blue circles)  $L$ -valley  $g$  factors in the conduction (positive for large  $D$ ) and valence (negative for large  $D$ ) bands in PbS (upper panel) and PbSe (lower panel) NCs extracted from the tight-binding calculations using Eq. (6). Red and blue lines show, respectively, longitudinal and transverse  $g$  factors computed within anisotropic (solid lines) and isotropic (dashed lines)  $\mathbf{k} \cdot \mathbf{p}$  theory with parameters extracted from the tight-binding model (Table I).

where  $E_g$  is the band gap,  $P$  is the interband momentum matrix element,  $m_0$  is the free-electron mass, the coefficients  $\alpha_{c(v)}$  stem from the contributions of the remote bands to the conduction- and valence-band energy dispersion, and  $\Delta$  is the three-dimensional Laplace operator.

Within the isotropic model, the electron states can be characterized by the value of the total angular momentum  $F$  and an additional quantum number  $p$  related to the parity of the states. The dispersion equation for these states is given in the Supplemental Material [34]. The ground electron states are characterized by the angular momentum  $F = 1/2$  and  $p = +1$  (odd parity), and the ground hole states have  $F = 1/2$  and  $p = -1$  (even parity). All the confined states are  $(2F + 1)$ -fold degenerate with respect to the projection  $F_z$  of the total angular momentum. Their wave functions written in bispinor form are

$$|F, p, n, F_z\rangle = \begin{pmatrix} f_{F-\frac{p}{2}, p}(\frac{r}{R}) \hat{\Omega}_{F, F_z}^{F-\frac{p}{2}} \\ i p g_{F+\frac{p}{2}, p}(\frac{r}{R}) \hat{\Omega}_{F, F_z}^{F+\frac{p}{2}} \end{pmatrix}, \quad (8)$$

where  $\hat{\Omega}_{F, F_z}^\ell$  are the spherical spinors [45] and  $f_{\ell p}, g_{\ell p}$  are the normalized radial functions [34].

To compute the  $g$  factors we follow Ref. [30] and add to the Hamiltonian (7) the following term,

$$\begin{aligned} \delta H &= \frac{e}{2c} (\mathbf{A}\mathbf{v} + \mathbf{v}\mathbf{A}) \\ &= \frac{e\mathbf{B}}{2c} \begin{pmatrix} -\frac{2i\alpha_c m_0}{\hbar^2} \mathbf{r} \times \nabla & \frac{P}{\hbar} (\mathbf{r} \times \boldsymbol{\sigma}) \\ \frac{P}{\hbar} (\mathbf{r} \times \boldsymbol{\sigma}) & \frac{2i\alpha_v m_0}{\hbar^2} \mathbf{r} \times \nabla \end{pmatrix}, \quad (9) \end{aligned}$$

where  $\mathbf{v}$  is the velocity operator [44]. We used the symmetric gauge  $\mathbf{A} = \frac{\mathbf{B} \times \mathbf{r}}{2}$  for the vector potential  $\mathbf{A}$  along with the additional electron and hole effective  $g$ -factor tensors with the nonzero components  $g_{0xx}^\eta = g_{0yy}^\eta = g_{0r}^\eta$ ,  $g_{0zz}^\eta = g_{0l}^\eta$ , responsible for the contributions of remote bands, to yield

$$H_{\text{iso}}(\mathbf{B}) = \mu_B \mathbf{B} \begin{pmatrix} \frac{1}{2} \hat{g}_0^c \boldsymbol{\sigma} + \frac{2m_0}{\hbar^2} \alpha_c \mathbf{L} & \frac{P}{\hbar} (\mathbf{r} \times \boldsymbol{\sigma}) \\ \frac{P}{\hbar} (\mathbf{r} \times \boldsymbol{\sigma}) & \frac{1}{2} \hat{g}_0^v \boldsymbol{\sigma} - \frac{2m_0}{\hbar^2} \alpha_v \mathbf{L} \end{pmatrix}, \quad (10)$$

where  $\mathbf{L} = -i\mathbf{r} \times \nabla$  and  $\mathbf{B} \hat{g}_0^\eta \boldsymbol{\sigma} = \sum_{\alpha, \beta} B_\alpha g_{0\alpha\beta}^\eta \sigma_\beta = \sum_\alpha B_\alpha g_{0\alpha\alpha}^\eta \sigma_\alpha$ .

We use the variables  $g_{0r}^\eta, g_{0l}^\eta$  as adjustable parameters to reproduce the  $g$  factors of the bulk PbS and PbSe, calculated in the tight-binding model (see, e.g., the Supplemental Material of Ref. [46]), from the following relations,

$$g_{l(r), \text{bulk}}^\eta = g_{0l(r)}^\eta \pm \frac{4P^2}{E_g m_0}, \quad (11)$$

where the sign of the second term is positive for  $\eta = c$  and negative for  $\eta = v$ . The values  $g_{l(r), \text{bulk}}^\eta$  and  $P$  are given in Table I. One can see that the tight-binding model gives very good agreement with the experimental values of the bulk  $g$  factors in PbS and PbSe. Note that, in Ref. [47], the contributions of remote bands to the  $g$  factors were omitted, as the second term in Eqs. (11) (13.1 for PbS and 33.4 for PbSe, by the absolute value) prevails in determining the bulk  $g$  factors. However, in NCs, the  $g$  factors are renormalized (in the first order, as a result of the quantum confinement energy being added to the band gap) and the contributions of remote bands become important.

TABLE I. Experimental and calculated (tight-binding, this work) bulk PbS and PbSe  $g$  factors, band gaps, and parameters of the isotropic  $\mathbf{k} \cdot \mathbf{p}$  model. Signs of experimental  $g$  factors have been corrected according to Ref. [48].

	PbS		PbSe	
	TB	Expt.	TB	Expt.
$g_l^v$	-9.624		-24.197	$-16.1 \pm 1.7^a$
$g_l^c$	-9.995	$-13 \pm 3^b$	-31.453	$-32 \pm 7^a$
$g_t^c$	10.136		25.992	$16.6 \pm 1^a$
$g_t^v$	11.053	$12 \pm 3^b$	31.265	$27 \pm 7^a$
$E_g$ (4.2 K), eV	0.294	$0.286^c$	0.213	$0.165^c$
$E_g$ (300 K), eV		$0.37\text{--}0.40^c$		$0.26\text{--}0.29^c$
$\alpha_v m_0 / \hbar^2$	2.635		2.674	
$\alpha_c m_0 / \hbar^2$	2.472		2.320	
$2P^2 / m_0$ , eV	1.926		3.555	

<sup>a</sup>Reference [49].

<sup>b</sup>Reference [50].

<sup>c</sup>Reference [51].

The matrix elements of the Hamiltonian (10) between conduction- (valence-) band states  $|c, F_z\rangle \equiv |\frac{1}{2}, +1, 0; F_z\rangle$  ( $|v, F_z\rangle \equiv |\frac{1}{2}, -1, 0; F_z\rangle$ ), Eq. (8), can be calculated explicitly. They are reduced to one-dimensional integrals containing the radial functions [34]. Linear-in- $\mathbf{B}$  terms give the values of the renormalized  $g$  factor in the conduction band

$$g_{t,l}^c = \int_0^R dr r^2 \left( g_{0+,l}^c f_{0+}^2(r) - \frac{8P}{3\hbar} r f_{0+}(r) g_{1+}(r) - \left[ \frac{g_{0+,l}^v}{3} + \frac{8\alpha_v m_0}{3\hbar^2} \right] g_{0+}^2(r) \right), \quad (12)$$

and in the valence band

$$g_{t,l}^v = \int_0^R dr r^2 \left( g_{0-,l}^v g_{0-}^2(r) - \frac{8P}{3\hbar} r f_{1-}(r) g_{0-}(r) - \left[ \frac{g_{0-,l}^c}{3} - \frac{8\alpha_c m_0}{3\hbar^2} \right] f_{1-}^2(r) \right). \quad (13)$$

In Fig. 3 the results of the calculations within the  $\mathbf{k} \cdot \mathbf{p}$  model according to Eqs. (12) and (13) are shown in dashed lines. The  $\mathbf{k} \cdot \mathbf{p}$  parameters used in calculations are given in Table I. The agreement with the tight-binding results is within the accuracy of the definition of the  $g$  factors extracted from the atomistic calculations. When NC shapes are varied [34], then the  $g$  factors obtained from the  $\mathbf{k} \cdot \mathbf{p}$  model overlap with the distribution of  $g$  factors in NCs of different shape, caused by shape-sensitive valley mixing [36]. However, the shape sensitivity of the valley mixing has relatively little effect on the values of the  $g$  factors. In Fig. 3 we also present the results of the anisotropic  $\mathbf{k} \cdot \mathbf{p}$  model described in detail in the Supplemental Material [34]. The only significant outcome of the anisotropic model is the nonvanishing difference in renormalizations of the longitudinal and transverse  $g$  factors.

However, this difference is small compared to the renormalizations themselves.

### III. CONCLUSIONS

To conclude, in this paper we have approached the calculation of  $g$  factors for the carriers confined in PbS and PbSe NCs from two different standpoints. On one hand, we utilized the empirical tight-binding method to obtain  $g$  factors of carrier states split at zero magnetic field by valley mixing and classified with respect to irreducible representations of the NC point group. On the other hand, we derived analytical equations for renormalizations of bulk carrier  $g$  factors due to the effect of quantum confinement in a NC using a single-valley effective  $\mathbf{k} \cdot \mathbf{p}$  Hamiltonian. We compared the outcomes of the two calculations by mapping the tight-binding results onto a single valley. This allowed us to express  $g$  factors of the carrier states, split by valley mixing and classified with respect to irreducible representations of the NC point group, in terms of the single-valley longitudinal and transverse  $g$  factors and to conclude that the sensitivity of valley mixing to the NC shape, while significant for zero-field splittings, has relatively little effect on carrier  $g$  factors.

### ACKNOWLEDGMENTS

The authors are indebted to D. R. Yakovlev for helpful discussions. The work of S.V.G. was supported by NSF through DMR-2100248. The work of I.D.A. was supported by Russian Science Foundation under Grant No. 22-72-00121 (numerical calculations). The work of M.O.N. was supported by Russian Science Foundation under Grant No. 19-12-00051 (analytical theory and symmetry analysis). I.D.A. also thanks the Foundation for Advancement of Theoretical Physics and Mathematics “BASIS.”

- 
- [1] L. Sun, J. J. Choi, D. Stachnik, A. C. Bartnik, B.-R. Hyun, G. G. Malliaras, T. Hanrath, and F. W. Wise, Bright infrared quantum-dot light-emitting diodes through inter-dot spacing control, *Nat. Nanotechnol.* **7**, 369 (2012).
- [2] V. Sukhovatkin, S. Hinds, L. Brzozowski, and E. H. Sargent, Colloidal quantum-dot photodetectors exploiting multiexciton generation, *Science* **324**, 1542 (2009).
- [3] W. A. Tisdale, K. J. Williams, B. A. Timp, D. J. Norris, E. S. Aydil, and X.-Y. Zhu, Hot-electron transfer from semiconductor nanocrystals, *Science* **328**, 1543 (2010).
- [4] L. Gao, L. N. Quan, F. P. G. de Arquer, Y. Zhao, R. Munir, A. Proppe, R. Quintero-Bermudez, C. Zou, Z. Yang, M. I. Saidaminov, O. Voznyy, S. Kinger, Z. Lu, S. O. Kelley, A. Amassian, J. Tang, and E. H. Sargent, Efficient near-infrared light-emitting diodes based on quantum dots in layered perovskite, *Nat. Photonics* **14**, 227 (2020).
- [5] H. Lu, Z. Huang, M. S. Martinez, J. C. Johnson, J. M. Luther, and M. C. Beard, Transforming energy using quantum dots, *Energy Environ. Sci.* **13**, 1347 (2020).
- [6] *Colloidal Quantum Dot Optoelectronics and Photovoltaics*, edited by G. Konstantatos and E. H. Sargent (Cambridge University Press, Cambridge, UK, 2013).
- [7] C. R. Kagan, E. Lifshitz, E. H. Sargent, and D. V. Talapin, Building devices from colloidal quantum dots, *Science* **353**, aac5523 (2016).
- [8] A. R. Kirmani, J. M. Luther, M. Abolhasani, and A. Amassian, Colloidal quantum dot photovoltaics: Current progress and path to gigawatt scale enabled by smart manufacturing, *ACS Energy Lett.* **5**, 3069 (2020).
- [9] D. Loss and D. P. DiVincenzo, Quantum computation with quantum dots, *Phys. Rev. A* **57**, 120 (1998).
- [10] A. Imamoglu, D. D. Awschalom, G. Burkard, D. P. DiVincenzo, D. Loss, M. Sherwin, and A. Small, Quantum Information Processing Using Quantum Dot Spins and Cavity QED, *Phys. Rev. Lett.* **83**, 4204 (1999).
- [11] R. J. Warburton, Single spins in self-assembled quantum dots, *Nat. Mater.* **12**, 483 (2013).
- [12] G. Cao, H.-O. Li, G.-D. Yu, B.-C. Wang, B.-B. Chen, X.-X. Song, M. Xiao, G.-C. Guo, H.-W. Jiang, X. Hu, and G.-P. Guo, Tunable Hybrid Qubit in a GaAs Double Quantum Dot, *Phys. Rev. Lett.* **116**, 086801 (2016).

- [13] G. D. Scholes, Selection rules for probing biexcitons and electron spin transitions in isotropic quantum dot ensembles, *J. Chem. Phys.* **121**, 10104 (2004).
- [14] V. M. Huxter, V. Kovalevskij, and G. D. Scholes, Dynamics within the exciton fine structure of colloidal CdSe quantum dots, *J. Phys. Chem. B* **109**, 20060 (2005).
- [15] G. D. Scholes, J. Kim, C. Y. Wong, V. M. Huxter, P. S. Nair, K. P. Fritz, and S. Kumar, Nanocrystal shape and the mechanism of exciton spin relaxation, *Nano Lett.* **6**, 1765 (2006).
- [16] Z. Zhang, Z. Jin, H. Ma, Y. Xu, X. Lin, G. Ma, and X. Sun, Room-temperature spin coherence in zinc blende CdSe quantum dots studied by time-resolved Faraday ellipticity, *Phys. E* **56**, 85 (2014).
- [17] R. Hu, D. R. Yakovlev, P. Liang, G. Qiang, C. Chen, T. Jia, Z. Sun, M. Bayer, and D. Feng, Origin of two Larmor frequencies in the coherent spin dynamics of colloidal CdSe quantum dots revealed by controlled charging, *J. Phys. Chem. Lett.* **10**, 3681 (2019).
- [18] Z. Wu, Y. Zhang, R. Hu, M. Jiang, P. Liang, Q. Yang, L. Deng, T. Jia, Z. Sun, and D. Feng, Hole-acceptor-manipulated electron spin dynamics in CdSe colloidal quantum dots, *J. Phys. Chem. Lett.* **12**, 2126 (2021).
- [19] M. J. Fernée, P. Tamarat, and B. Lounis, Cryogenic single-nanocrystal spectroscopy: Reading the spectral fingerprint of individual CdSe quantum dots, *J. Phys. Chem. Lett.* **4**, 609 (2013).
- [20] C. Sinito, M. J. Fernée, S. V. Goupalov, P. Mulvaney, P. Tamarat, and B. Lounis, Tailoring the exciton fine structure of cadmium selenide nanocrystals with shape anisotropy and magnetic field, *ACS Nano* **8**, 11651 (2014).
- [21] J. Schrier and K. B. Whaley, Tight-binding  $g$ -factor calculations of CdSe nanostructures, *Phys. Rev. B* **67**, 235301 (2003).
- [22] P. Chen and K. B. Whaley, Magneto-optical response of CdSe nanostructures, *Phys. Rev. B* **70**, 045311 (2004).
- [23] A. Tadjine, Y.-M. Niquet, and C. Delerue, Universal behavior of electron  $g$ -factors in semiconductor nanostructures, *Phys. Rev. B* **95**, 235437 (2017).
- [24] M. A. Semina, A. A. Golovatenko, and A. V. Rodina, Influence of the spin-orbit split-off valence band on the hole  $g$  factor in semiconductor nanocrystals, *Phys. Rev. B* **104**, 205423 (2021).
- [25] J. C. Johnson, K. A. Gerth, Q. Song, J. E. Murphy, A. J. Nozik, and G. D. Scholes, Ultrafast exciton fine structure relaxation dynamics in lead chalcogenide nanocrystals, *Nano Lett.* **8**, 1374 (2008).
- [26] L. Turyanska, J. H. Blokland, U. Elfurawi, O. Makarovskiy, P. C. M. Christianen, and A. Patané, Photoluminescence of PbS nanocrystals at high magnetic fields up to 30 T, *Phys. Rev. B* **82**, 193302 (2010).
- [27] R. D. Schaller, S. A. Crooker, D. A. Bussian, J. M. Pietryga, J. Joo, and V. I. Klimov, Revealing the Exciton Fine Structure of PbSe Nanocrystal Quantum Dots Using Optical Spectroscopy in High Magnetic Fields, *Phys. Rev. Lett.* **105**, 067403 (2010).
- [28] Y. Kim, Z. Hu, I. D. Avdeev, A. Singh, A. Singh, V. Chandrasekaran, M. O. Nestoklon, S. V. Goupalov, J. A. Hollingsworth, and H. Htoon, Interplay of bright triplet and dark excitons revealed by magneto-photoluminescence of individual PbS/CdS quantum dots, *Small* **17**, 2006977 (2021).
- [29] I. Kang and F. W. Wise, Electronic structure and optical properties of PbS and PbSe quantum dots, *J. Opt. Soc. Am. B* **14**, 1632 (1997).
- [30] A. A. Kiselev, E. L. Ivchenko, and U. Rössler, Electron  $g$  factor in one- and zero-dimensional semiconductor nanostructures, *Phys. Rev. B* **58**, 16353 (1998).
- [31] G. Allan and C. Delerue, Confinement effects in PbSe quantum wells and nanocrystals, *Phys. Rev. B* **70**, 245321 (2004).
- [32] A. N. Poddubny, M. O. Nestoklon, and S. V. Goupalov, Anomalous suppression of valley splittings in lead salt nanocrystals without inversion center, *Phys. Rev. B* **86**, 035324 (2012).
- [33] G. Bir and G. Pikus, *Symmetry and Strain-Induced Effects in Semiconductors* (Wiley, New York, 1974).
- [34] See Supplemental Material at <http://link.aps.org/supplemental/10.1103/PhysRevB.107.035414> for details of the calculations, results of atomistic calculations of different QD shapes, details of the calculations in the isotropic and anisotropic  $\mathbf{k} \cdot \mathbf{p}$  model, and the explicit form of the matrices transforming the basis functions of independent valleys to the basis of irreducible representations of the group  $T_d$ .
- [35] I. D. Avdeev, Shape effect on the valley splitting in lead selenide nanowires, *Phys. Rev. B* **99**, 195303 (2019).
- [36] I. D. Avdeev, M. O. Nestoklon, and S. V. Goupalov, Exciton fine structure in lead chalcogenide quantum dots: Valley mixing and crucial role of intervalley electron-hole exchange, *Nano Lett.* **20**, 8897 (2020).
- [37] Note that in Ref. [52] the effective Hamiltonian is written in terms of the matrices  $J_\gamma^3$ .
- [38] J.-M. Jancu, R. Scholz, F. Beltram, and F. Bassani, Empirical  $spds^*$  tight-binding calculation for cubic semiconductors: General method and material parameters, *Phys. Rev. B* **57**, 6493 (1998).
- [39] A. Svane, N. E. Christensen, M. Cardona, A. N. Chantis, M. van Schilfgaarde, and T. Kotani, Quasiparticle self-consistent GW calculations for PbS, PbSe, and PbTe: Band structure and pressure coefficients, *Phys. Rev. B* **81**, 245120 (2010).
- [40] M. Graf and P. Vogl, Electromagnetic fields and dielectric response in empirical tight-binding theory, *Phys. Rev. B* **51**, 4940 (1995).
- [41] C. R. Bealing, W. J. Baumgardner, J. J. Choi, T. Hanrath, and R. G. Hennig, Predicting nanocrystal shape through consideration of surface-ligand interactions, *ACS Nano* **6**, 2118 (2012).
- [42] H. Choi, J.-H. Ko, Y.-H. Kim, and S. Jeong, Steric-hindrance-driven shape transition in PbS quantum dots: Understanding size-dependent stability, *J. Am. Chem. Soc.* **135**, 5278 (2013).
- [43] M. O. Nestoklon and S. V. Goupalov, Exciton interaction with acoustic phonons in PbS nanocrystals, *Phys. Rev. B* **106**, 045306 (2022).
- [44] S. V. Goupalov, E. L. Ivchenko, and M. O. Nestoklon, Optical transitions, exciton radiative decay, and valley coherence in lead chalcogenide quantum dots, *Phys. Rev. B* **106**, 125301 (2022).
- [45] D. A. Varshalovich, A. N. Moskalev, and V. K. Khersonskii, *Quantum Theory of Angular Momentum* (World Scientific, Singapore, 1988).
- [46] E. Kirstein, D. R. Yakovlev, M. M. Glazov, E. A. Zhukov, D. Kudlacik, I. V. Kalitukha, V. F. Sapega, G. S. Dimitriev, M. A. Semina, M. O. Nestoklon, E. L. Ivchenko, N. E. Kopteva, D. N. Dirin, O. Nazarenko, M. V. Kovalenko, A. Baumann, J. Höcker, V. Dyakonov, and M. Bayer, The Landé factors of electrons and holes in lead halide perovskites: Universal dependence on the band gap, *Nat. Commun.* **13**, 3062 (2022).

- [47] J. O. Dimmock and G. B. Wright, Band edge structure of PbS, PbSe, and PbTe, *Phys. Rev.* **135**, A821 (1964).
- [48] P. J. Lin and L. Kleinman, Energy bands of PbTe, PbSe, and PbS, *Phys. Rev.* **142**, 478 (1966).
- [49] J. Y. Leloup, B. Sapoval, and G. Martinez, Knight shift in multivalley semiconductors. II. Determination of the hyperfine coupling constants in *n*- and *p*-type PbSe and PbTe, *Phys. Rev. B* **7**, 5276 (1973).
- [50] S. Rabbii, Investigation of energy-band structures and electronic properties of PbS and PbSe, *Phys. Rev.* **167**, 801 (1968).
- [51] W. H. Strehlow and E. L. Cook, Compilation of energy band gaps in elemental and binary compound semiconductors and insulators, *J. Phys. Chem. Ref. Data* **2**, 163 (1973).
- [52] E. L. Ivchenko and G. E. Pikus, *Superlattices and Other Heterostructures: Symmetry and Optical Phenomena*, 1st ed. (Springer, Berlin, 2005).